Extension of the thermal porosimetry method to high gas pressure for nanoporosimetry estimation

Yves Jannot, Alain Degiovanni, Marc Camus

Extension of the thermal porosimetry method to high gas pressure for nanoporosimetry estimation

Y. Jannot, A. Degiovanni, M. Camus

Université de Lorraine, LEMTA (UMR 7563), ENSEM, 2 Avenue de la Forêt de Haye, BP 90161, 54505 Vandoeuvre-lès-Nancy cedex, France

CNRS, LEMTA (UMR 7563), BP 90161, 54505 Vandoeuvre-lès-Nancy cedex, France

Abstract

Standard pore size determination methods like mercury porosimetry, nitrogen sorption, microscopy or X-ray tomography are not suited to highly porous, low density and thus very fragile materials. For this kind of materials, a method based on thermal characterization has been developed in a previous study. This method has been used with air pressure varying from 10^{-1} to 10^{5} Pa for materials having a thermal conductivity less than $0.05\ \mathrm{W\,m^{-1}\,K^{-1}}$ at atmospheric pressure. It enables the estimation of pore size distribution between 100 nm and 1 mm. In this paper, we present a new experimental device enabling thermal conductivity measurement under gas pressure up to 10^{6} Pa, enabling the estimation of the volume fraction of pores having a 10 nm diameter. It is also demonstrated that the main thermal conductivity models (Parallel, Series, Maxwell, Bruggeman, Self-consistent) lead to the same estimation of the pore size distribution as the extended parallel model (EPM) presented in this paper and then used to process the experimental data.
Three materials with thermal conductivities at atmospheric pressure ranging from $0.014\ \mathrm{W\,m^{-1}\,K^{-1}}$ to $0.04\ \mathrm{W\,m^{-1}\,K^{-1}}$ are studied. The thermal conductivity measurements results obtained with the three materials are presented and the corresponding pore size distributions between 10 nm and 1 mm are presented and discussed.

Keywords: Insulating material, nano-porosimetry, pore size distribution, thermal conductivity, pressure, vacuum.

Y. Jannot, A. Degiovanni, A. Aubert, F. Lechleiter, In-plane thermal diffusivity measurement of thin plates by the transient fin method, Review of Scientific Instruments, 89, 2018.

Nomenclature

a, b	Coefficients	
C	Constant depending on gas nature	mbar.m.K
d	Pore size	m
d_x	Relative uncertainty on parameter x	
I	Current intensity	A
J	Number of values in an experimental curve	
K	Number of noised curves simulated	
N	Number of ranges of pore size	
P	Pressure	mbar
p_x	Parameter number x	
r	Random number between -1 and 1	
S	Surface of the heating element	m^2
S_x	Reduced sensitivity to the parameter x	
T	Temperature	K
U	Voltage applied to the heating element	V
α	Fraction of the gas associated to continuous transfer (CSP model)	
β	Fraction of the solid associated to continuous transfer (CSP model)	
δ	Mean free path	m
ε_x	Volume fraction of the x phase	
η	Constant in the air thermal conductivity model	
γ	Constant of the EPM model	
λ_x	Thermal conductivity of the x phase	$W.m^{-1}.K^{-1}$
ρ	Density	$kg.m^{-3}$
Subscripts		
air	Air	
atm	Atmospheric pressure	
c	Contacts	
cp	Continuous paths	
exp	Experimental	
i	i^{th} air phase	
j	j^{th} point of the conductivity curve	
k	k^{th} noised conductivity curve	
mod	Modeled	
v	Vacuum	
s	Solid	

Introduction

Thermal porosimetry is a method developed for the estimation of pore size distribution in a porous medium. This method takes place as a complement to other classical methods such as mercury porosimetry[1-3], gas sorption[4-6] or imagery[7-8]. It is based on the processing of thermal conductivity measurements performed on a sample set in an enclosure with variable air pressure. For highly porous and insulating materials, the thermal conductivity of the sample is sensitive to the thermal conductivity of the air and thus to the size of the containing pore[9]. O.J. Lee et al.[10] already used this sensitivity to deduce information about the pores size from thermal conductivity measurements under various air pressure values. Felix et al.[11] develop a method to estimate pore size distribution between 100 nm and 1 mm by processing thermal conductivity measurements realized under gas pressures varying from 1 to 10^5 Pa. They also validate the method with materials having a thermal conductivity lower than $0.05\ W\ m^{-1}\ K^{-1}$.

In this paper we present a new experimental device enabling the measurement of the thermal conductivity of a porous medium under a gas pressure up to 10^6 Pa, extending the estimation of the pore size distribution between 10 nm and 1 mm.
Then the results obtained with three materials with thermal conductivities ranging from $\lambda = 0.014\ \mathrm{W\,m^{-1}\,K^{-1}}$ to $0.04\ \mathrm{W\,m^{-1}\,K^{-1}}$ under normal gas pressure are given. Finally the pore size distributions of each material between 10 nm and 1 mm are presented.

Theoretical background

Thermal conductivity of the air

A highly porous material is mainly composed of air which thermal conductivity is a function of both its pressure and the size of its containing cavity. Indeed, if the mean free path of gaseous molecules is high related to the mean distance between the cavity walls, those molecules only interact with the walls, so that the heat conduction property is governed by the pore size, this is called the Knudsen effect. As a consequence, pore size is an important parameter in the equation of the thermal conductivity of the air that is confined into a pore. For spherical pores, that equation comes under the form[9]:

$$\lambda_{air}(P,d) = \frac{\lambda_0}{1+2\eta\, Kn(P,d)} \qquad (1)$$

With: λ_0 Thermal conductivity of the air at atmospheric pressure (0.026 W.m^{-1}.K^{-1})
η Constant, $\eta = 1.5$ for air[9]

The Knudsen number $Kn(P,d)$ is calculated by:

$$Kn(P,d) = \frac{\delta}{d} \qquad (2)$$

With: d Pore diameter (m)
δ Mean free path, its value for air is[12]: $\delta(P) = 2.27 \times 10^{-5}\ \frac{T}{P}$ (3)
T Temperature (K)
P Air pressure (Pa)

Fig. 1 shows that the thermal conductivity of the air does not vary in the same pressure range for different values of d. It also shows that thermal conductivity of air in the pores with a 10 nm diameter varies significantly only for gas pressure values between 10^5 Pa and 10^6 Pa.

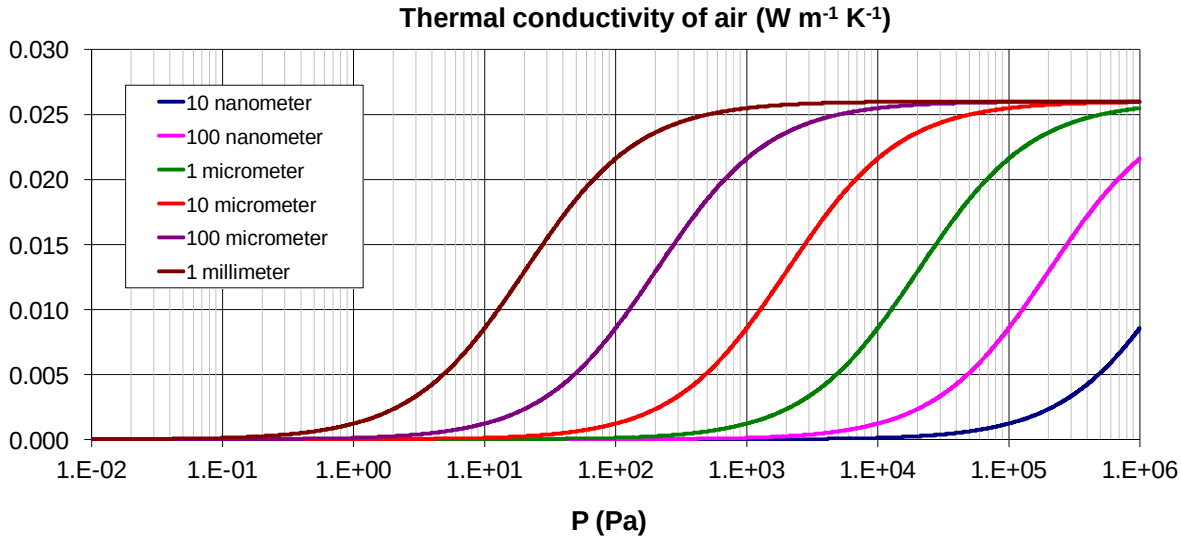

Figure 1: Thermal conductivity of air vs gas pressure for different pore diameters

Thermal conductivity of porous media

The material is considered as a heterogeneous porous medium which global porosity ratio is $\varepsilon_{air} = 1 - \varepsilon_s$, composed of a solid phase characterized by its thermal conductivity λ_s and N fluid phases (air). Each fluid phase correspond to a class of pore diameter d_i with thermal conductivity $\lambda_{air,i}$ and volume fraction $\varepsilon_{air,i}$.
Several models can be used to predict the thermal conductivity of the equivalent homogeneous medium $\lambda_{mod} = f(\varepsilon_s, \lambda_s, \varepsilon_{air,i}, \lambda_{air,i})$. According to Felix et al[11] , the most suited ones for low density thermal insulators are the parallel model (PM) and a combined serial/parallel (CSP) model developed by these authors[11]. The later one was developed to represent the thermal conductivity of materials which thermal conductivity verifies:

$$\lambda_{P=1atm} - \lambda_{P<10^{-2}mbar} > \varepsilon_s \lambda_s \quad (4)$$

In this case, the parallel model can no longer represent the thermal conductivity on all the pressure range.
In fact, to estimate the pores size distribution, one only needs the form of the curve $\lambda = f(P)$, the amplitude enabling the estimation of the thermal conductivity of the solid phase.
It is thus possible to process only the reduced thermal conductivities curves defined as:

$$\lambda^* = \frac{\lambda_{mod} - \lambda_0}{\lambda_\infty - \lambda_0} \quad (5)$$

Where λ_∞ is the thermal conductivity for $P \to \infty$ and λ_0 is the thermal conductivity for $P \to 0$.
We will show that for low density porous materials ($\varepsilon_{air} > 0{,}80$), all the main thermal conductivity models leads to similar curves for λ^*. It is the reason why the thermal porosity method is a robust method, leading to the same estimation of the pore size distribution whatever the model used. On the contrary, the estimated value of the solid phase thermal conductivity highly depends on the model used.
We have thus chosen the model closer to the physics of the considered materials, i.e. the parallel model, hence:

$$\lambda^* = \frac{\lambda_{mod} - \lambda_0}{\lambda_\infty - \lambda_0} = \frac{\lambda_\parallel - \lambda_{0\parallel}}{\lambda_{\infty\parallel} - \lambda_{0\parallel}} \quad (6)$$

Thus: $\lambda_{mod} = \frac{\lambda_\parallel - \lambda_{0\parallel}}{\lambda_{\infty\parallel} - \lambda_{0\parallel}} (\lambda_\infty - \lambda_0) + \lambda_0$ (7)

With for the parallel model: $\lambda_\parallel = \varepsilon_s \lambda_s + \sum_i \varepsilon_i \lambda_i$ (8)

And: $\lambda_{0\parallel} = \varepsilon_s \lambda_s$ (9)

Thus: $\lambda_{mod} = (\lambda_\infty - \lambda_0)/(\lambda_{\infty\parallel} - \lambda_{0\parallel}) \sum_i \varepsilon_i \lambda_i + \lambda_0$ (10)

The model used for the estimation called the extended parallel model (EPM) can then be expressed as:

$$\lambda_{mod} = \gamma \sum_i \varepsilon_i \lambda_i + \lambda_0 \quad (11)$$

Where γ and λ_0 are two unknown parameters to be identified.
The figures represent the simulated thermal conductivities and their reduced values as a function of the gas pressure for 8 models and for 3 types of products representing the products that will be further studied and a cellular concrete.
The models are:

- The Maxwell model[13]: (1)
- The parallel model: (2)

- The series model: (3)
- The Bruggeman models[14]: (4), (5) and (6), the last one being the average of (4) and (5)
- The self-consistent model[15] (7)
- The combined series-parallel model CSP[11].

The expressions of the thermal conductivity given by these models are presented in the Appendix.
For the comparison, the considered typical porous materials have two pores sizes, which are described in Table 1. To be more realistic, we have used the properties that have been estimated from experimental curves.

Table 1: Characteristics of the typical materials considered for the simulations

	Nano-T	Super-insulator	Pavapor	Cellular concrete
d_1	10^{-3}	10^{-7}	10^{-4}	10^{-4}
d_2	10^{-7}	10^{-8}	10^{-5}	10^{-7}
ε_s	0.123	0.1	0.104	0.35
ε_1	0.03	0.45	0.566	0.5
ε_2	0.844	0.45	0.33	0.15
λ_s	0.2	0.33	0.26	0.4
α	0.964	0.958	0.896	0.99989
β	0.599	0.4	0.544	0.96388

The figures 2 to 4 show that the thermal conductivities simulated with the different models are quite different but that the reduced ones are rather the same for three first materials having high porosities: Nano-T, super-insulator and Pavapor.

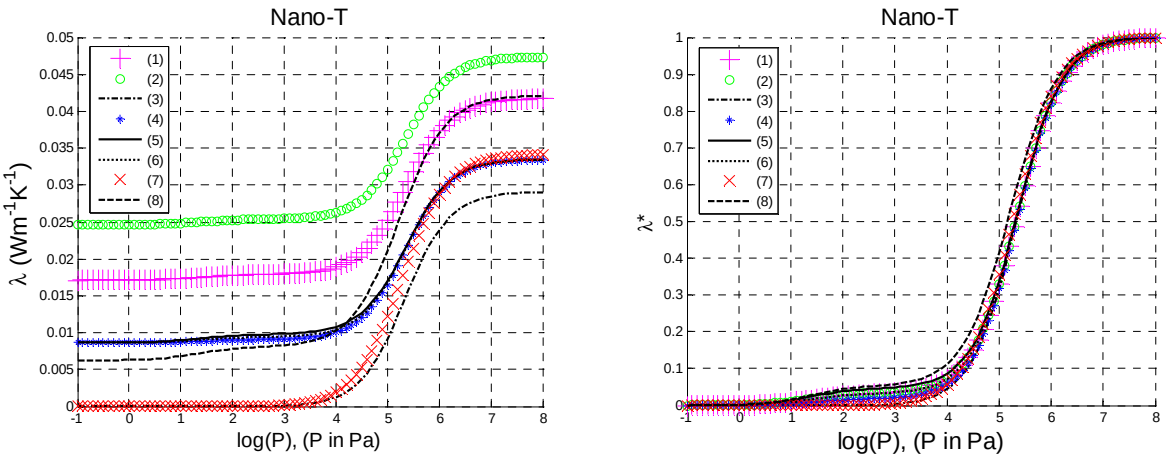

Figure 2: Thermal conductivity λ (and reduced one λ^*) of Nano-T, simulated by different models

One can wonder if the method could be extended to lower porosity materials such as cellular concrete (with 0.65 porosity) which characteristics are given in Table 1. The eight models have been tested on this material. Figure 5 shows that in this case even the reduced thermal conductivity curves obtained with the different models cannot be assimilated to a unique curve. Thus, the estimated pore size distribution will depends on the thermal conductivity model used for the estimation. The thermal porosimetry technique is thus only suited to high porosity insulating materials with a porosity greater than 0.80.

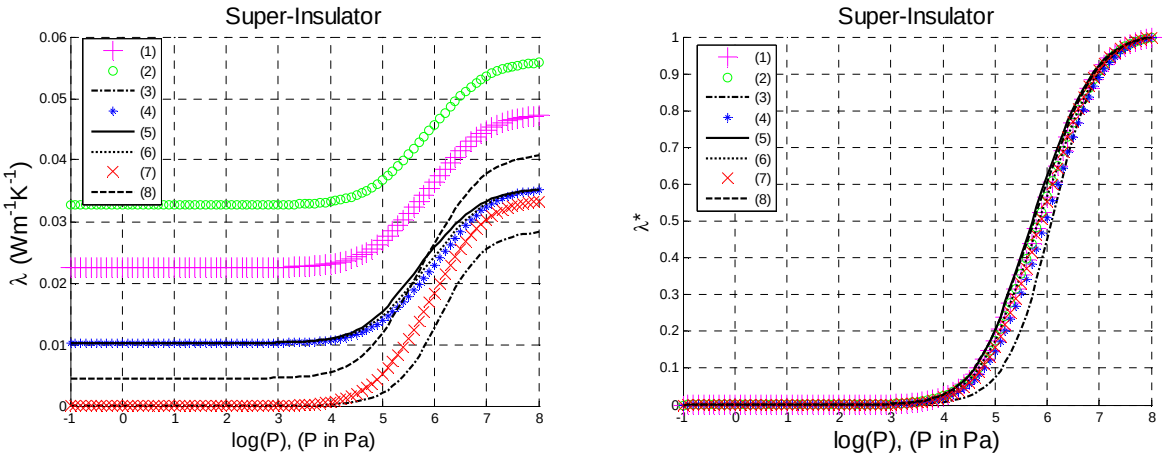

Figure 3: Thermal conductivity λ (and reduced one λ) of super-insulator, simulated by different models*

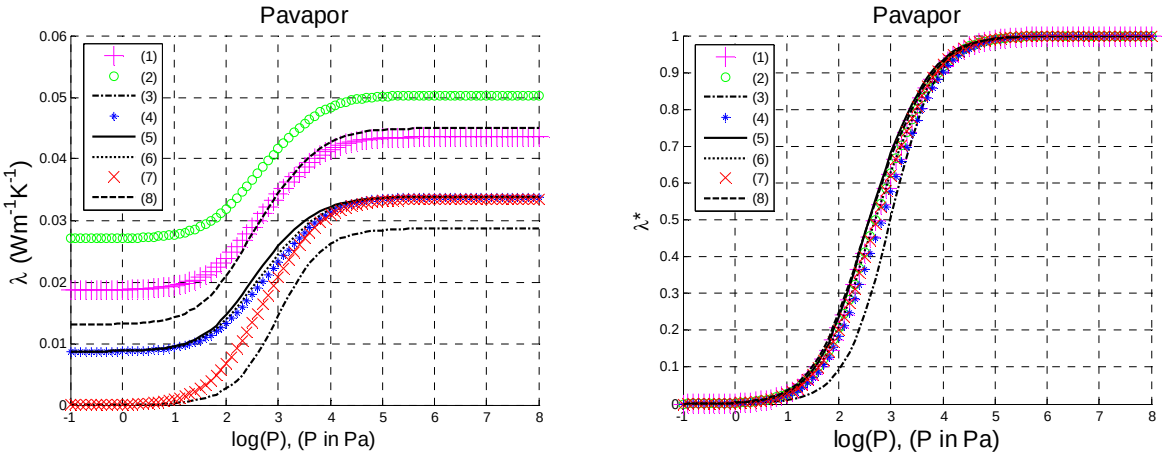

Figure 4: Thermal conductivity λ (and reduced one λ) of Pavapor, simulated by different models*

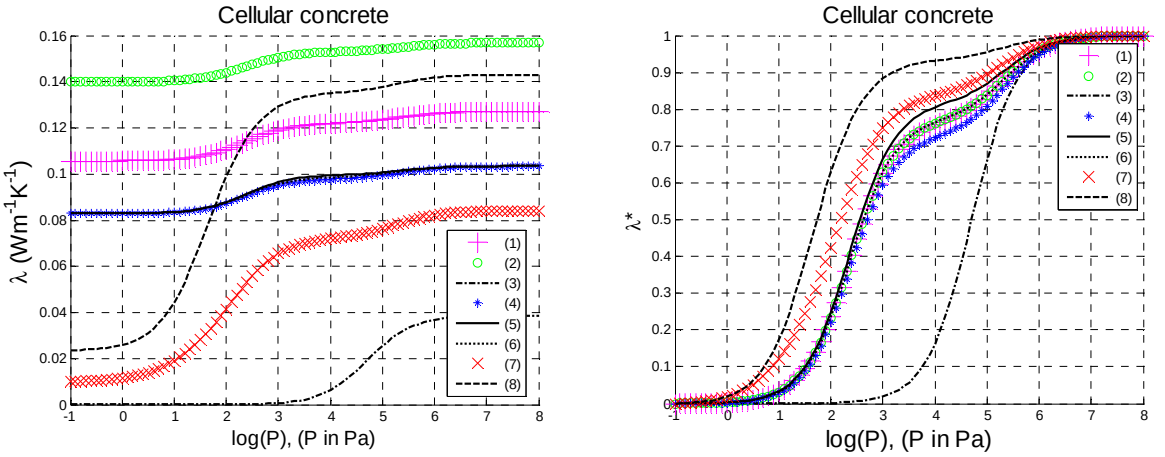

Figure 5: Thermal conductivity λ (and reduced one λ) of cellular concrete, simulated by different models*

The presented models only take into account the conduction heat transfer. Nevertheless, radiation heat transfer may be significant especially in low density porous media. In fact, since all the experiments are carried out at the same temperature and radiation is independent on gas

pressure, the contribution of the radiation heat transfer is included in the estimated parameter independent on the gas pressure, i.e. the thermal conductivity of the solid phase. Particularly, when the equivalent thermal conductivity is extrapolated for a null gas pressure, the obtained value takes into account both the conduction in the solid phase and the radiation.

Materials and methods

Materials and devices

This study has been carried out on insulating materials for which density and global porosity have been measured using a helium pycnometer device[16]:

- A super-insulating material with a density $\rho = 116.8\ \mathrm{kg\,m^{-3}}$ and a global porosity $\varepsilon_{air} = 0.901$.
- "Nano-T" commercialized by Final Materials that is an insulating material design for high temperature applications with a density $\rho = 247.7\ \mathrm{kg\,m^{-3}}$ and a global porosity $\varepsilon_{air} = 0.877$.
- "Pavapor" that is a fibrous wood-based material commercialized by Pavatex with a density $\rho = 152.9\ \mathrm{kg\,m^{-3}}$ and a global porosity $\varepsilon_{air} = 0.896$.

Thermal conductivity measurements have been done using the centered hot plate method[17] with $100 \times 100\ \mathrm{mm^2}$ cross section samples. The measurement device (see figure 6) has been placed inside a chamber in which pressure is controlled between 10^{-1} and 10^{6} Pa. Fig. 1 shows that the thermal conductivity of the air stops decreasing under 10^{-1} Pa if the pores size is lower than 1 mm. Apparently, the considered materials have not any pore greater than 1 mm, so measuring conductivities at lower pressures than 10^{-1} Pa would not bring any useful information.

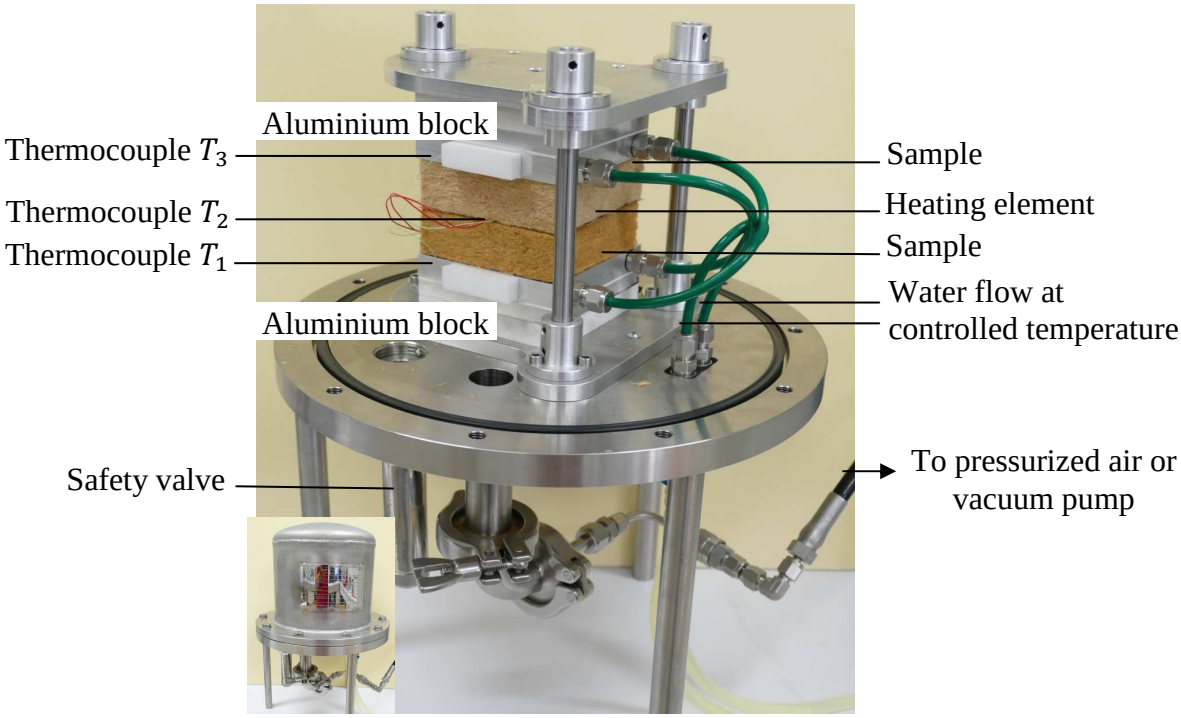

Figure 6: View of the measurement device

Sensitivity analysis

The choice of the number N of ranges of pore sizes is based on a sensitivity analysis developed

by Felix et al[11]. According to their conclusions, the value $N = 6$ was chosen with the following mean diameter values of the pores: 10 nm, 100 nm, 1µm, 10 µm, 100 µm and 1 mm.

Estimation method

The first step is to measure the thermal conductivity of the materials under different pressures varying between 10^{-1} and 10^{6} Pa. Typically, the thermal conductivity is measured for at least four different pressures for each pressure decade, such as represented on figure 7 giving an example of a measurement set.

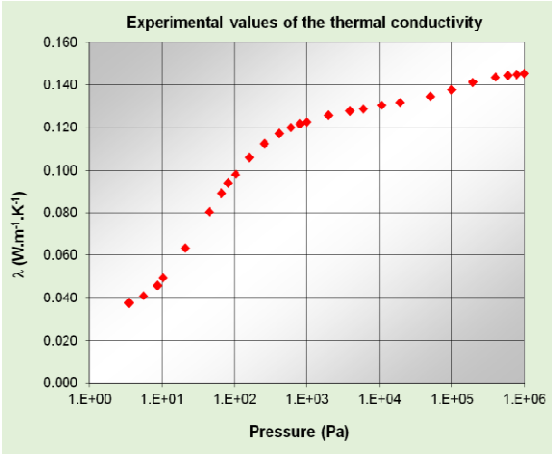

Figure 7: Example of thermal conductivity measurements used for the estimation of pore size distribution

The inversion process is built on the principle of minimization of the sum of the quadratic differences, given by relation (12), between the thermal conductivity experimental data $\lambda_{exp,i}$ and the modeled values $\lambda_{mod,i}$ calculated using relation (11). The minimization is achieved using the Levenberg-Marquardt algorithm. The thermal conductivity EPM model requires to estimate 8 parameters: λ_0, γ and six values of ε_{air_i}. The minimization constraints are the followings:

$$\min \sum_{j=i}^{J} \left(\lambda_{mod,i} - \lambda_{exp,i}\right)^2 \quad (12)$$

$$0 \leq \varepsilon_{air,i} \leq 1 \quad (13)$$

$$\sum_{i=1}^{6} \varepsilon_{air,i} = 1 - \varepsilon_s \quad (14)$$

Standard deviations of the estimated parameters

Thermal conductivity measurements using the hot plate method are deduced from the expression:

$$\lambda_{exp} = \frac{R_{el}}{S} \frac{e\, I^2}{\Delta T} \quad (15)$$

With:

e Samples' thickness (m)

R_{el} Electrical resistance of the heating element (Ω)

I Current intensity passing through the heating element (A)

S Surface of the heating element (m^2)

ΔT Temperature difference between the heated surface of the sample and the constant temperature surface (°C)

Two kinds of errors can be done on these measurements:

- A systematic error on each experimental value of the thermal conductivity which depends on the knowledge of the thickness e (± 1%) and of the surface S (± 2%), which introduce a

constant deviation equal to ± 3% on the measured values.

- A random error, different for each point due to the accuracy of the current I measuring device (± 1%) and of the temperature acquisition chain which is evaluated at 0.1 °C for a ΔT of 10 °C representing a ± 1% deviation. The total random deviation is so estimated at ± 2% of the measured value.

The error on the global porosity ratio using the Helium pycnometer[16] has been considered constant and equal to ± 2%. Finally, the uncertainty on pressure measurements has been evaluated at ± 5% of the measured value.

Standard deviations of the estimated parameters (λ_0 ,γ, $\varepsilon_{air,i}$) have been calculated by a statistical method. Modeled thermal conductivities λ_{mod} have first been computed taking the estimated parameters as nominal values and considering the biased value $\varepsilon_s + d\varepsilon_s$ of the solid volume fraction ε_s (so that the uncertainty on the global porosity ratio ε_{air} is considered);

Then, the obtained values of the thermal conductivities and the experimental pressure values are noised K times as describes by relations (16) and (17):

$$P_{k,j} = P_j + r_{k,j}\, dP \tag{16}$$

$$\lambda_{k,j} = \lambda_{mod} + d\lambda + r'_{k,j}\, d\lambda' \tag{17}$$

Where: $1 < k < K$ and: $1 < j < J$

With:

J	Number of experimental points of the thermal conductivity curve $\lambda_{exp}(P)$
K	Number of simulated thermal conductivity curves $\lambda_k(P)$
$r_{k,j}$, $r'_{k,j}$	Random number (uniform density of probability between –1 and +1)
$d\lambda$	Maximum value of the systematic error on λ due to the errors on e and S
$d\lambda'$	Uncertainty due to random error on I and ΔT
dP	Uncertainty due to random error on P

The K noised curves $\lambda_k(P)$ have been considered as ‘numerical’ experiments and a set of optimal parameters (λ_0 ,γ, $\varepsilon_{air,i}$) has been estimated for each curve.

Finally the mean values and the standard deviations of the K estimated values for each parameter have been calculated. To have a good statistic representation, K has been set to 1000.

Results and discussion

The results obtained by processing the thermal conductivity measurements of the three studied materials are presented in this part. Measurements have then been processed considering the global porosity ratio as a known parameter measured by Helium pycnometry.

Figure 8 representing the thermal conductivity vs gas pressure shows a very good fitting of the experimental points by the EPM model, with very low residues centered on the null value. Figure 9 representing the volume fraction for each pore size class shows that a porous material must contain a high percentage of nanopores to be super-insulating. The estimated pores size distribution for Pavapor (wooden wool) in the range 10 to 100 µm is in agreement with the pore size of wood which mean value is around 40 µm. It could also be noticed that the low volume fraction of pore with diameter in the range 100 µm - 1 mm for super insulator materials could be interpreted by the existence of point defects inside the material or at the contact between the material and the heating resistance on one hand, and between the material and the thermostated blocks on the other hand. Nevertheless, the corresponding volume fraction is quite low in each case.

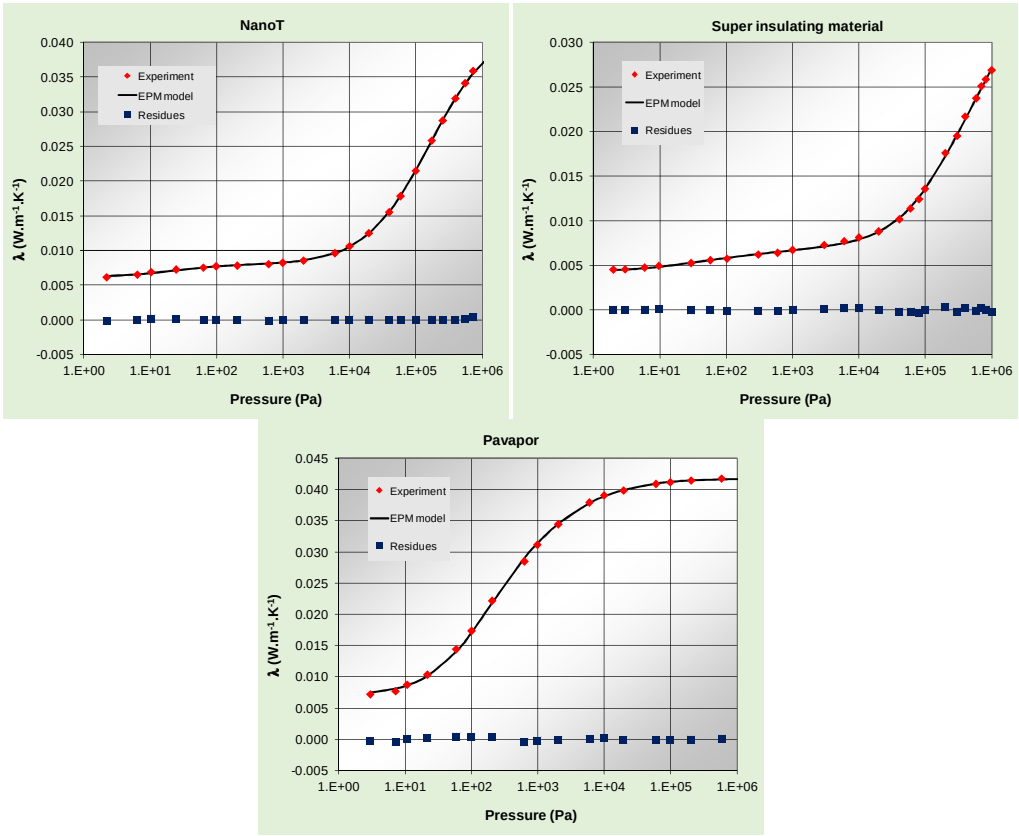

Figure 8: Thermal conductivities (experiment, model and residues) vs gas pressure

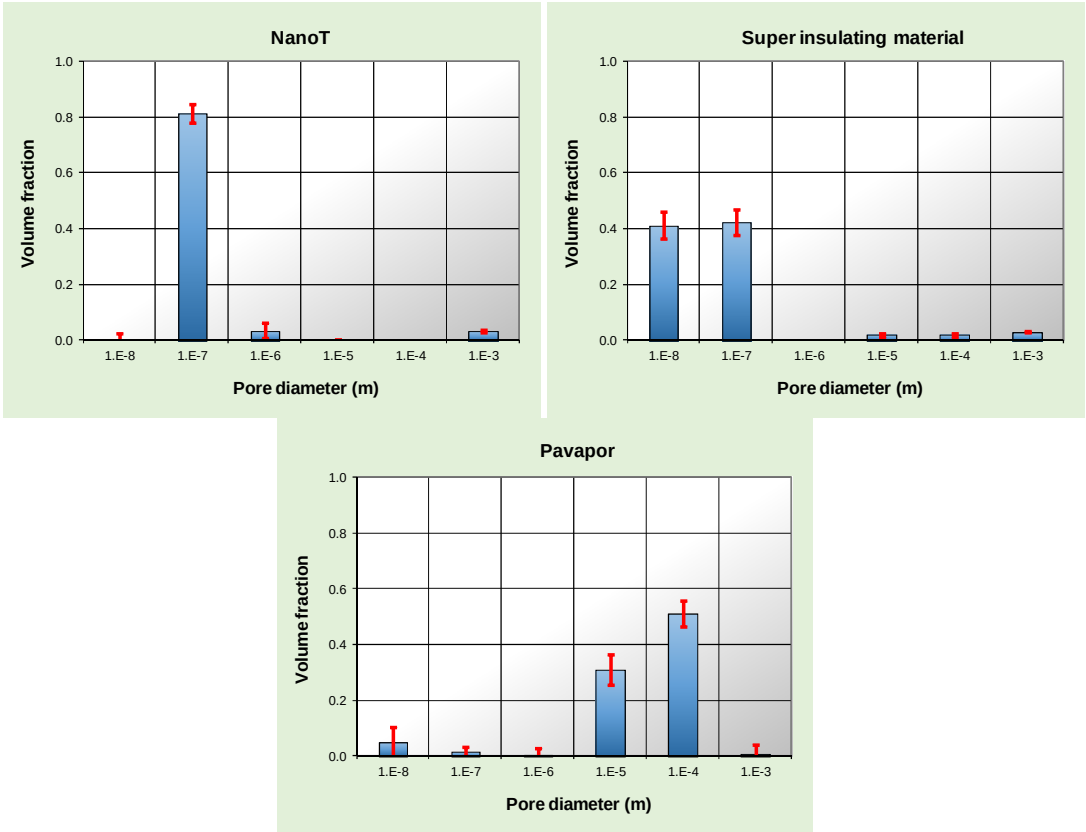

Figure 9: Estimated pore size distributions

Conclusion

We showed that it is possible to determine the distribution of the open pores sizes of a low density porous material by a thermal method.
Working under gaseous pressure up to 10 bars makes it possible to detect pore sizes as low as 10 nm, so that the pore size characterization of super-insulators becomes possible.
The main advantages of this method are the followings:

- with regard to the classical methods, such as the mercury porosimetry or the nitrogen sorption, it enables to obtain directly the size of pores and not the size of the opening of pores.
- there is no mechanical constraint applied on the sample during the measurement, so that it may be used for fragile materials with very high porosities (up to 99%).
- the method is robust, since it is independent from the model.

Its main disadvantages are the followings:

- it requires a great number of thermal conductivity measurements (around 20) so that it may take a long time.
- it is only suited to materials having a high porosity (greater than 0.8).

References

[1] Washburn E.W., "Note on a method of determining the distribution of pore sizes in a porous material", Proc. Natl. Acad. Sci., **7**, 115, (1921).

[2] Pirard R. , Alié C. and Pirard J.P., "Characterization of porous texture of hyperporous materials by mercury porosimetry using densification equation", Powder Technology **128**, 242-247, (2002).

[3] Rigby S.P., Fletcher R.S. and Riley S.N., "Characterization of porous solids using integrated nitrogen sorption and mercury porosimetry", Chemical Engineering Science **59**, 41-51, (2004).

[4] Saleh K. and Guigon P., "Caractérisation et analyse des poudres – Propriétés physiques des solides divisés", Techniques de l'Ingénieur J2251, (2009).

[5] Barrett E.P., Joyner L.G. and Halenda P.P., "The determination of pore volume and area distributions in porous substances. I. Computations from nitrogen isotherms", J. Am. Chem. Soc. **73**, 373–380, (1951).

[6] Rouquerol F., Denoyel R., Luciani L., Rouquerol J. and Llewellyn P., "Texture des matériaux pulvérulents ou poreux", Techniques de l'Ingénieur, P1050, (2003).

[7] Lux J., "Comportement thermique macroscopique de milieux fibreux réels anisotropes : étude basée sur l'analyse d'images tridimensionnelles", Thèse de doctorat, Université Bordeaux 1, (2005).

[8] Kaemmerlen A., "Transfert de chaleur à travers les isolants thermiques du bâtiment", Thèse de doctorat, Université Henri Poincaré Nancy I, (2009).

[9] Collishaw P.G. and Evans J.R.G., "An assessment of expressions for the apparent thermal conductivity of cellular materials", Journal of Materials Science, **29**, 2661-2273 (1994).

[10]Lee O.-J., Lee K.-H., Yim T., Kim S.Y and Yoo K.K., "Determination of mesopore size of aerogels from thermal conductivity measurements", Journal of Non-Crystalline Solids, **298**, 287-292 (2002).

[11]Félix V., Jannot Y. and Degiovanni A., "Thermoporosimetry: a new method to estimate pore size distribution in highly porous insulating materials", Review of Scientific Instruments, **83**, (2012).

[12] Langlais C. and Klarsfeld S., "Isolation thermique à température ambiante. Transfert de chaleur", Techniques de l'ingénieur, BE 9859, (2004).

[13] Maxwell J.C., "A treatise on electricity and magnetism", Oxford, Clarendon Press, (1873).

[14] Maxwell Garnett J.C., "Colours in metal glasses and in metallic films", Philos. Trans. Roy. Soc., **A203**, 385–420, (1904).

[15] Bruggeman D.A.G., "Dielectric constant and conductivity of mixture of isotropic materials", Annalen. Physik, **24**, 636-679, (1953).

[16] Bal H., Jannot Y., Quenette N., Chenu A. and Gaye S., "Water content dependence of the porosity, density and thermal capacity of laterite based bricks with millet waste additive", Construction & Building Materials, **31**, 144-150 (2012).

[17] Jannot Y., Félix V. and Degiovanni A., "A centered hot plate method for measurement of thermal properties of thin insulating materials", Measurement Science and Technology, **21**, (2010).

Appendix

Expressions of the thermal conductivity λ_{mod} given by different models for a porous media with global porosity ratio $\varepsilon_{air} = 1 - \varepsilon_s$, composed of a solid phase characterized by its thermal conductivity λ_s and its volume fraction ε_s, and N fluid phases (air). Each fluid phase correspond to a class of pore diameter d_i with thermal conductivity $\lambda_{air,i}$ and volume fraction $\varepsilon_{air,i}$.

Parallel model (2):

$$\lambda_{mod} = \varepsilon_s\lambda_s + \varepsilon_1\lambda_1 + (1 - \varepsilon_s - \varepsilon_1)\lambda_2 \quad \text{(A1)}$$

Serial model (3):

$$\lambda_{mod} = \left(\frac{\varepsilon_s}{\lambda_s} + \frac{\varepsilon_1}{\lambda_1} + \frac{1-\varepsilon_s-\varepsilon_1}{\lambda_2}\right)^{-1} \quad \text{(A2)}$$

Combined serial/parallel model (CSP), (8):

$$\lambda_{mod} = \left[\frac{\beta\varepsilon_s+\alpha(1-\varepsilon_s)}{\lambda_{cp}} + \frac{(1-\beta)\varepsilon_s+(1-\alpha)(1-\varepsilon_s)}{\lambda_c}\right] \quad \text{(A3)}$$

With: $\lambda_{cp} = \frac{\beta\varepsilon_s\lambda_s+\alpha[\varepsilon_1\lambda_1+(1-\varepsilon_s-\varepsilon_1)\lambda_2]}{\beta\varepsilon_s+\alpha(1-\varepsilon_s)}$ (A4)

And: $\lambda_c = \frac{(1-\beta)\varepsilon_s\lambda_s+(1-\alpha)[\varepsilon_1\lambda_1+(1-\varepsilon_s-\varepsilon_1)\lambda_2]}{(1-\beta)\varepsilon_s+(1-\alpha)(1-\varepsilon_s)}$ (A5)

Maxwell (1):

$$\lambda_{mod} = \lambda_s \frac{\varepsilon_s+\varepsilon_1\frac{3\lambda_1}{2\lambda_s+\lambda_1}+(1-\varepsilon_s-\varepsilon_1)\frac{3\lambda_2}{2\lambda_s+\lambda_2}}{\varepsilon_s+\varepsilon_1\frac{3\lambda_s}{2\lambda_s+\lambda_1}+(1-\varepsilon_s-\varepsilon_1)\frac{3\lambda_s}{2\lambda_s+\lambda_2}} \quad \text{(A6)}$$

Self-consistent (7):

$$\lambda_{mod} = 3\lambda_{mod}\left[\varepsilon_s\frac{\lambda_s}{2\lambda_{mod}+\lambda_s} + \varepsilon_1\frac{\lambda_1}{2\lambda_{mod}+\lambda_1} + (1-\varepsilon_s-\varepsilon_1)\frac{\lambda_2}{2\lambda_{mod}+\lambda_2}\right] \quad \text{(A7)}$$

Bruggemann(4), (5) and (6):

$$\lambda_{mod_4} = \lambda_s\,{\varepsilon_s}^{3/2} + \lambda_1\left[(\varepsilon_s+\varepsilon_1)^{3/2} - {\varepsilon_s}^{3/2}\right] + \lambda_2\left[1-(\varepsilon_s+\varepsilon_1)^{3/2}\right] \quad \text{(A8)}$$

$$\lambda_{mod_5} = \lambda_s\,{\varepsilon_s}^{3/2} + \lambda_1\left[1-(1-\varepsilon_1)^{3/2}\right] + \lambda_2\left[(1-\varepsilon_1)^{3/2} - {\varepsilon_s}^{3/2}\right] \quad \text{(A9)}$$

$$\lambda_{mod_6} = \frac{\lambda_{mod_4}+\lambda_{mod_5}}{2} \quad \text{(A10)}$$